

Structure of Dark Matter Halos in Warm Dark Matter models and in models with Long-Lived Charged Massive Particles

Ayuki Kamada, Naoki Yoshida

*Kavli Institute for the Physics and Mathematics of the Universe, University of Tokyo, Kashiwa,
Chiba 277-8583, Japan*

Department of Physics, University of Tokyo, Tokyo 113-0033, Japan

ayuki.kamada@ipmu.jp

Kazunori Kohri

*Cosmology group, Theory Center, IPNS, KEK, and The Graduate University for Advanced Study
(Sokendai), Tsukuba, 305-0801, Japan*

and

Tomo Takahashi

Department of Physics, Saga University, Saga 840-8502, Japan

ABSTRACT

We study the formation of non-linear structures in Warm Dark Matter (WDM) models and in a Long-Lived Charged Massive Particle (CHAMP) model. CHAMPs with a decay lifetime of about 1 yr induce characteristic suppression in the matter power spectrum at subgalactic scales through acoustic oscillations in the thermal background. We explore structure formation in such a model. We also study three WDM models, where the dark matter particles are produced through the following mechanisms: i) WDM particles are produced in the thermal background and then kinematically decoupled; ii) WDM particles are fermions produced by the decay of thermal heavy bosons; and iii) WDM particles are produced by the decay of non-relativistic heavy particles. We show that the linear matter power spectra for the three models are all characterised by the comoving Jeans scale at the matter-radiation equality. Furthermore, we can also describe the linear matter power spectrum for the Long-Lived CHAMP model in terms of a suitably defined characteristic cut-off scale k_{Ch} , similarly to the WDM models. We perform large cosmological N -body simulations to study the non-linear growth of structures in these four models. We compare the halo mass functions, the subhalo mass functions, and the radial distributions of subhalos in simulated Milky Way-size halos. For the characteristic cut-off scale $k_{\text{cut}} = 51 h \text{ Mpc}^{-1}$, the subhalo abundance

($\sim 10^9 M_{\text{sun}}$) is suppressed by a factor of ~ 10 compared with the standard Λ CDM model. We then study the models with $k_{\text{cut}} \simeq 51, 410, 820 h \text{ Mpc}^{-1}$, and confirm that the halo and the subhalo abundances and the radial distributions of subhalos are indeed similar between the different WDM models and the Long-Lived CHAMP model. The result suggests that the cut-off scale k_{cut} not only characterises the linear power spectra but also can be used to predict the non-linear clustering properties. The radial distribution of subhalos in Milky Way-size halos is consistent with the observed distribution for $k_{\text{cut}} \sim 50 - 800 h \text{ Mpc}^{-1}$; such models resolve the so-called “missing satellite problem”.

Subject headings: cosmology: theory - early universe - dark matter

1. Introduction

The precise measurement of the cosmic microwave background (CMB) anisotropies established the standard $\Lambda + \text{Cold Dark Matter}$ (Λ CDM) cosmology (Komatsu et al. 2011). Observations of the large-scale structure of the Universe, such as the galaxy power spectra from the Sloan Digital Sky Survey (SDSS) also confirmed its success in predicting the large scale structures of the Universe (e.g. Tegmark et al. (2004); Reid et al. (2010); Percival et al. (2010)).

The validity of the Λ CDM model on the galactic and the subgalactic scales has long been caught up in debate. Moore et al. (1999) argue that the number of dark matter subhalos is $10 - 100$ times larger than the number of satellites observed around the Milky Way (Kravtsov 2010). The so-called “missing satellite problem” has been revisited in a somewhat quantitative context (Boylan-Kolchin et al. 2011; Lovell et al. 2012; Boylan-Kolchin et al. 2012). For example, Boylan-Kolchin et al. (2011) argue that, in the Λ CDM model, ~ 10 most massive subhalos in a galactic halo are too concentrated to be consistent with the kinematic data for the bright Milky Way satellites. Also, observations of the rotation velocities of galaxies using the 21 cm line by Papastergis et al. (2011) show that the abundance of galaxies with observed velocity width $w = 50 \text{ km s}^{-1}$ is ~ 8 times lower than predicted in the Λ CDM model.

It is often suggested that WDM models resolve the apparent problems on subgalactic scales (Bode et al. 2001). WDM particles have non-negligible velocity dispersions, which act as an effective “pressure” of the WDM fluid. Essentially, the subgalactic-scale density fluctuations are suppressed. The resultant matter power spectrum is quickly reduced around the cut-off scale that is determined by the velocity dispersion. Motivated by the recent interest in this problem, several authors study the structure formation in WDM models (Dunstan et al. 2011; Schneider et al. 2012; Menci et al. 2012).

Constraints on WDM models can be obtained from astronomical observations. Observations of Lyman- α forests are often used for the purpose (Viel et al. 2005; Boyarsky et al. 2009). Absorption features in quasar spectra reflect the number density of neutral hydrogen, from which we can esti-

mate the matter power spectrum along the line of sight, even at large wavenumbers $k \sim 10 h \text{ Mpc}^{-1}$. WDM models have also interesting implications for the cosmic reionization (Barkana et al. 2001; Yoshida et al. 2003; Gao & Theuns 2007). The formation of the first objects, and hence the production of ionizing photons, are delayed in WDM models. On the other hand, WDM models could help the completion of the cosmic reionization. Yue & Chen (2012) suggest that the reduced number of subhalos in WDM models makes the recombination of ionized hydrogens inefficient and results in earlier completion of the cosmic reionization. It is clearly important to study the clustering properties in WDM models in both linear and non-linear evolution regimes.

There are also renewed interest in particle physics. Several candidates for WDM are suggested in particle physics models beyond the Standard Model, such as light gravitinos (Kawasaki et al. 1997), sterile neutrinos (see Kusenko (2009) for a review and references) and superWIMPs (Cembranos et al. 2005). It is important to notice that WDM particles can be produced via different mechanisms. Nevertheless, the above constraints from astronomical observations are focused on a single quantity, e.g., the mass of WDM particle in a specific model. It is unclear if such constraints can be applied to WDM models with different production mechanisms. Detailed comparisons of a wide class of models are clearly needed.

In this paper, we also consider a Long-Lived CHAMP model. Throughout this paper, we assume that CHAMPs have an elementary charge, either positive or negative. CHAMPs are generally realized in models beyond the Standard Model of particle physics. One such example is a slepton, a superpartner of leptons in supersymmetric models. S sleptons as the lightest supersymmetry particles (LSPs) are stable when R-parity is conserved. The abundance of such stable CHAMPs, however, is severely constrained by the searches in deep sea water (see Beringer et al. (2012) for a review and references). CHAMPs can also be unstable; a CHAMP decay into neutral dark matter and other decay products including at least one charged particle. For example, the stau can be the next lightest supersymmetric particle (NLSP) when the gravitino is the LSP (Buchmüller et al. 2006). It is well-known that CHAMPs could affect the big bang nucleosynthesis (BBN) reaction rates and thus change the abundance of light elements (Pospelov 2007; Kohri & Takayama 2007; Kaplinghat & Rajaraman 2006; Cyburt et al. 2006; Steffen 2007; Hamaguchi et al. 2007; Kawasaki et al. 2007; Jedamzik 2008a,b; Jittoh et al. 2011). Several authors (Sigurdson & Kamionkowski 2004; Kohri & Takahashi 2010) suggest the possibility that CHAMPs with a lifetime about 1 yr can act effectively as WDM through acoustic oscillations in the thermal background. We study the effect of the oscillations on the matter power spectrum.

We calculate the linear evolution of the matter density fluctuations for the three WDM models and the Long-Lived CHAMP model. We show that the comoving Jeans scale at the matter-radiation equality characterises the linear matter power spectra in the three WDM models well. We use the obtained linear matter power spectra as initial conditions of N -body simulations to follow the non-linear evolution of the matter distribution. We compare the halo mass functions, the subhalo mass functions, and the radial distributions of subhalos in Milky Way-size halos to discuss the clustering properties in the WDM models and in the Long-Lived CHAMP model. We show that

these statistics are similar when the cut-off scale is kept the same. We find that the WDM models and the Long-Lived CHAMP model with the characteristic cut-off scale $k_{\text{cut}} \sim 50 - 800 h \text{ Mpc}^{-1}$ resolve the so-called “missing satellite problem”.

The rest of this paper is organised as follows. In Sec. 2, we summarize three WDM models and a Long-Lived CHAMP model we consider. Then, we introduce the common cut-off scale k_{cut} which characterises the linear matter power spectra in these models. In Sec. 3, after describing the details of N -body simulations, we show simulation results and discuss their implications. Specifically, we mention the similarity of these models with the same cut-off and the possibility that CHAMPs behave like WDMs and resolve the “missing satellite problem”. Finally, in Sec. 4, concluding remarks are given.

Throughout this paper, we take the cosmological parameters that are given in Komatsu et al. (2011) as the *WMAP*+BAO+ H_0 Mean; $100\Omega_b h^2 = 2.255$, $\Omega_{\text{CDM}} h^2 = 0.1126$, $\Omega_\Lambda = 0.725$, $n_s = 0.968$, $\tau = 0.088$ and $\Delta_R^2(k_0) = 2.430 \times 10^{-9}$, while we replace the energy density of CDM $\Omega_{\text{CDM}} h^2$ by the energy density of WDM $\Omega_{\text{WDM}} h^2$ for the WDM models and by the energy density of neutral dark matter produced by the CHAMP decay for the Long-Lived CHAMP model.

2. WDM models and Long-Lived CHAMP model

In this section, we summarize three WDM models and a Long-Lived CHAMP model we consider in this paper. We describe production mechanisms of WDM particles in each model and show the exact shapes of the velocity distribution. In the following subsections, we focus on three WDM models to specify our discussion, although our results can be applied to any WDM models with the same shape of the velocity distribution. Then, we introduce the Jeans scale at the matter-radiation equality. The matter power spectra in the three WDM models with the same Jeans scale at the matter-radiation equality are very similar. Their initial velocity distributions affect the damping tail of the matter power spectra. We also describe the evolution of the linear matter density fluctuations in a Long-Lived CHAMP model. The matter power spectrum is truncated around the horizon scale at the time when CHAMPs decay. Interestingly, the resulting power spectrum appears similar to those in WDM models.

2.1. Thermal WDM

In this type of models, fermionic WDM particles are produced in the thermal background. They are decoupled from the thermal background as the Universe expands and cools. At the time of the decoupling, their momentum obeys the thermal distribution, that is, the Fermi-Dirac distribution. We consider the generalized Fermi-Dirac distribution,

$$f(p) = \frac{\beta}{e^{p/T_{\text{WDM}}} + 1}. \quad (1)$$

Here and in the following, p denotes the comoving momentum of WDM particles, and T_{WDM} is the effective temperature that characterises the comoving momentum of WDM particles. In the case of the light gravitino (Dine et al. 1996) and the thermally produced sterile neutrino (Olive & Turner 1982), T_{WDM} relates to the temperature of the left-handed neutrino T_ν through the conservation of the entropy, $T_{\text{WDM}} = \left(\frac{43/4}{g_{\text{dec}}}\right)^{1/3} T_\nu$ where g_{dec} is the effective number of the massless degrees of freedom at the decoupling from the thermal background. Note that β determines the overall normalization of the momentum distribution and $\beta = 1$ in the case of the gravitino and the thermally produced sterile neutrino. Dodelson & Widrow (1994) propose the sterile neutrino dark matter produced via active-sterile neutrino oscillations. In this case, the active neutrinos in the thermal background turn into the sterile neutrino via the coherent forward scattering (Cline 1992). The resultant momentum distribution of the sterile neutrino is given by the generalized Fermi-Dirac distribution (see Eq. (1)) with $T_{\text{WDM}} \simeq T_\nu$ and $\beta \propto \theta_m^2 M$ where θ_m is the active-sterile mixing angle and M is the mass of the sterile neutrino.

2.2. WDM produced by the thermal boson decay

There are models in which the Majorana mass of the sterile neutrino arises from the Yukawa coupling Y with a singlet boson (Shaposhnikov & Tkachev 2006; Petraki & Kusenko 2008). In these models, the singlet boson couples to the Standard Model Higgs boson through an extension of the Standard Models Higgs sector. The singlet Higgs boson has a vacuum expectation value (VEV) of the order of the electroweak scale when the electroweak symmetry breaks down. When the sterile neutrino is assumed to be WDM with a mass of an order of keV, the Yukawa coupling should be very small $Y \sim O(10^{-8})$. This small Yukawa coupling makes the singlet boson decay to the two sterile neutrinos when the singlet boson is relativistic and is in equilibrium with the thermal background. Here, it should be noted that the sterile neutrino model is one specific example. In WDM models, where relativistic bosonic particles in equilibrium with the thermal background decay into fermionic WDM particles through the Yukawa interaction, WDM particles have the same resultant momentum distribution (see Eq. (2) below). The resultant momentum distribution is obtained by solving the Boltzmann equation (Boyanovsky 2008),

$$f(p) = \frac{\beta}{(p/T_{\text{WDM}})^{1/2}} g_{5/2}(p/T_{\text{WDM}}) \quad (2)$$

where

$$g_\nu(x) = \sum_{n=1}^{\infty} \frac{e^{-nx}}{n^\nu}. \quad (3)$$

Here, we have ignored the low momentum cut-off that ensures the Pauli blocking, while it does not change our results. The effective temperature is given by $T_{\text{WDM}} = \left(\frac{43/4}{g_{\text{pro}}}\right)^{1/3} T_\nu$ with the effective number of massless degrees of freedom at the production of the sterile neutrino $g_{\text{pro}} \sim 100$. The

normalization factor β is determined by the Yukawa coupling Y and the mass of the singlet Higgs boson M , $\beta \propto Y^2 M^{-1}$. The velocity distribution have an enhancement $f_B \propto p^{-1/2}$ at the low momentum $p/T_{\text{WDM}} \ll 1$, since the sterile neutrinos with lower momenta are produced by the less boosted singlet boson, the decay rate of which is larger due to the absence of the time dilation. This enhancement indicates the “colder” (than the thermal WDM) property of the sterile neutrino dark matter produced by the decay of the singlet heavy boson.

2.3. WDM produced by the non-relativistic particle decay

In this type of models, a non-relativistic heavy particle decays into two particles, one or both of which become WDM. Supersymmetric theories realize this type of scenarios e.g. when the LSP is the gravitino and the NLSP is a neutralino. The relic abundance of the NLSP neutralino is determined at the time of chemical decoupling by the standard argument (Gondolo & Gelmini 1991; Griest & Seckel 1991). Eventually, the non-relativistic neutralinos decay into LSP gravitinos that become WDM. The particles produced by the decay of the moduli fields and of the inflaton fields are another candidates of this type of WDM (Lin et al. 2001; Hisano et al. 2001; Kawasaki et al. 2006; Endo et al. 2006; Takahashi 2008). When we assume the heavy particle decays in the radiation dominated era, the momentum distribution of the decay products is given by (Kaplinghat 2005; Strigari et al. 2007; Aoyama et al. 2011),

$$f(p) = \frac{\beta}{(p/T_{\text{WDM}})} \exp(-p^2/T_{\text{WDM}}^2), \quad (4)$$

where T_{WDM} is given by $T_{\text{WDM}} = P_{\text{cm}} a(t_d)/a(t_0)$ with the physical center-of-mass momentum P_{cm} , the scale factor $a(t)$ at the decay time t_d and at the present time t_0 . We have defined t_d as $H(t = t_d) = 1/2\tau$ where $H(t)$ is the Hubble parameter and τ is the lifetime of the heavy particle.

2.4. Jeans scale at the matter-radiation equality

Now, we introduce two quantities to characterise the property of WDM. One is the present energy density of WDM, $\Omega_{\text{WDM}} \equiv \frac{\rho_{\text{WDM}}}{\rho_{\text{crit}}}|_{t=t_0}$. Throughout this paper, we assume WDM particles account for all of the dark matter, letting $\Omega_{\text{WDM}} h^2 = 0.1126$. Another important physical scale is the comoving Jeans scale at the matter radiation equality t_{eq} ,

$$k_J = a \sqrt{\frac{4\pi G \rho_M}{\sigma^2}} \Big|_{t=t_{\text{eq}}} \quad (5)$$

with the gravitational constant G . Here, ρ_M is the matter density and σ^2 is the mean square of the velocity of the dark matter particles (see Eq. (8) below). Dark matter particles with $k_J \sim 100 - 1000 \text{ Mpc}^{-1}$ are usually called WDM and expected to resolve the “missing satellite problem”.

We note that, in the present paper, we do not consider whether or not a particular set of Ω_{WDM} and k_{J} is in a viable region of the respective model. One such example is the gravitino WDM, a representative of the Thermal WDM model (see subsection 2.1). This model has only two parameters, the effective number of the massless degrees of freedom at the decoupling g_{dec} and the gravitino mass $m_{3/2}$, to set Ω_{WDM} and k_{J} . When we assume $k_{\text{J}} \simeq 30 \text{ Mpc}^{-1}$, these two parameters are determined as $g_{\text{dec}} \simeq 1000$ and $m_{3/2} \simeq 1 \text{ keV}$. The effective number of the massless degrees of freedom at the decoupling of the gravitino is at most $g_{\text{dec}} \sim 200$ in the Minimal Supersymmetric Standard Model (MSSM), and hence, another mechanism such as entropy production is needed to explain the gravitino WDM (Ibe et al. 2011; Ibe & Sato 2012).

2.5. Linear matter power spectra and Normalized velocity distribution

We follow the evolution of the primordial adiabatic fluctuations for the three WDM models by modifying suitably the public software, CAMB (Lewis et al. 2000). We adopt the covariant multipole perturbation approach for the massive neutrino (Ma & Bertschinger 1995; Lewis & Challinor 2002). We replace the Fermi-Dirac distribution of the massive neutrino by the momentum distributions of the WDM models discussed above. Our approach is valid when the WDM particles are kinematically decoupled at the cosmic time of interest. The Jeans scale of interest is around $k_{\text{J}} \sim O(100) \text{ Mpc}^{-1}$. The primordial fluctuation of this wavenumber enters the horizon at $T \sim O(10) \text{ keV}$. In a large class of WDM models, WDM particles are kinematically decoupled before the QCD phase transition, $T_{\text{QCD}} \sim 100 \text{ MeV}$, and thus our calculation is valid.¹

For comparison, we calculate the normalized velocity distributions for the WDM models and the linear matter power spectra extrapolated to the present time $z = 0$. The results are shown in Fig. 1 for $k_{\text{J}} = 51 \text{ Mpc}^{-1}$, which correspond to $m_{3/2} \simeq 2 \text{ keV}$ for the thermally-produced gravitino WDM. Here, we have defined the dimensionless matter power spectra as,

$$\Delta(k) \equiv \frac{1}{2\pi^2} k^3 P(k) \quad (6)$$

with the matter power spectra $P(k)$.

The velocity distribution $g(v)$ is normalized as follows:

$$\int_0^\infty dv g(v) = 1, \quad (7)$$

¹There are variants of WDM models in which WDM particles are produced by the non-relativistic particle decay at late epochs. The matter power spectrum could be affected if the parent particles decay around the matter-radiation equality. In this case, the matter density during the radiation-dominated era is mostly contributed by the parent (cold) particles, rather than by the decay products, and then the density fluctuations of the cold, neutral parent particles can grow logarithmically. Note that the effect is more pronounced if the parent particles are charged (see subsection 2.6).

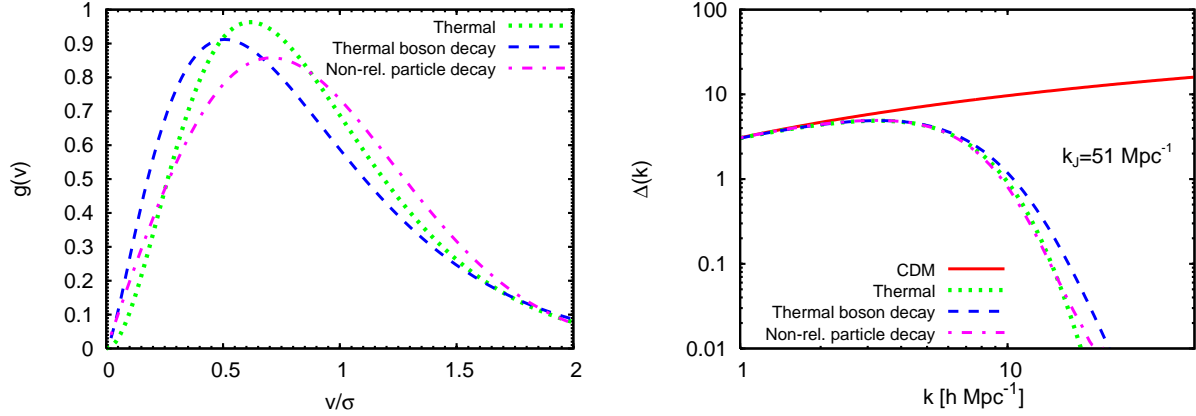


Fig. 1.— The normalized velocity distributions (left panel) and the dimensionless linear matter power spectra (right panel) for the standard CDM model and the three WDM models with $k_J = 51 \text{ Mpc}^{-1}$.

$$\int_0^\infty dv v^2 g(v) = \sigma^2 \quad (8)$$

with the variance (second moment) of the velocity σ^2 . Note that the first equation is normalized with respect to the present energy density of WDM, Ω_{WDM} , whereas the second equation relates the velocity variance to the comoving Jeans scale at the matter radiation equality k_J given by Eq. (5). One can then expect that the power spectra for the WDM models with the same Ω_{WDM} and k_J are very similar, as seen in Fig. 1. There, we see differences between the WDM models only in the damping tail of the power spectra at $k > 10 h \text{ Mpc}^{-1}$.

2.6. Long-Lived CHAMP and Cut-off scale

Sigurdson & Kamionkowski (2004) formulate the linearized evolution equations for fluctuations in a Long-Lived CHAMP model. They show that the subgalactic-scale matter density fluctuations are damped via a mechanism called “acoustic damping”. The comoving horizon scale at which CHAMP decays determines the cut-off scale of the matter power spectrum, which is defined by (Hisano et al. 2006; Kohri & Takahashi 2010)

$$k_{\text{Ch}} = aH|_{t=\tau_{\text{Ch}}}, \quad (9)$$

where H is the Hubble parameter and τ_{Ch} is the lifetime of CHAMP. Smaller-scale density fluctuations with $k > k_{\text{Ch}}$ enter the horizon before CHAMP decays and can not grow due to the acoustic oscillations of CHAMP in the thermal background. On the other hand, larger-scale density fluctuations with $k < k_{\text{Ch}}$ grow logarithmically even after entering the horizon due to the gravitational instability as the density fluctuations of CDM. We assume CHAMPs decay in the

radiation dominated era. Then the comoving horizon scale at $t = \tau_{\text{Ch}}$ is evaluated as,

$$k_{\text{Ch}} = 2.2 \text{ Mpc}^{-1} \times \left(\frac{\tau_{\text{Ch}}}{\text{yr}} \right)^{-1/2} \left(\frac{g_{\text{Ch}}}{3.363} \right)^{1/4} \quad (10)$$

where g_{Ch} is the effective number of massless degrees of freedom when CHAMP decays.

We need to consider three physical processes for the CHAMP model. First, we describe the neutralization of CHAMP. A positively charged particle may become neutral by forming a bound state with an electron e . Its binding energy is, however, almost the same as the hydrogen, $E_{b_e} \simeq 13.6 \text{ eV}$. Hence, the positively charged particle keeps charged until its decay, since we assume CHAMP decays in the radiation dominated era. A negatively charged particle may become neutral by forming a bound state with a proton p . Its binding energy $E_{b_p} \simeq 25 \text{ keV}$ is almost $m_{4\text{He}}/m_p \sim 2000$ times larger than E_{b_e} and hence is expected to make the negatively charged particle neutral at $T \sim 1 \text{ keV}$. However, Helium ^4He is produced through BBN, with which a negatively charged particle may form a binding state. Its binding energy $E_{b_{^4\text{He}}} \simeq 337 \text{ keV}$ is almost $(Z_{^4\text{He}}/Z_p)^2 \times m_{4\text{He}}/m_p \simeq 16$ times larger than E_{b_p} . It should be noted that even a negatively charged particle bound with a proton is wrested by ^4He through a charge-exchange reaction (Kamimura et al. 2009). Therefore, when the yield of CHAMP Y_{Ch} ($Y \equiv n/s$ with the number density n and the entropy density s) is smaller than the yield of the Helium $Y_{4\text{He}}$, almost every negatively charged particle forms a binding state with a helium nuclei, which has one positive elementary charge (Kohri & Takahashi 2010).

Second, the decay products of CHAMP may lead to energy injection to the thermal background. The resulting injection energy density is constrained from the photodissociation of BBN (Kawasaki et al. 2001) and CMB y - and μ - parameters (Hu & Silk 1993). However, models with CHAMP with almost the same mass with neutral dark matter are not severely constrained by BBN nor by CMB. We focus on such an “unconstrained” model. Note that the small mass splitting ensures the relatively long lifetime of CHAMP and the “coldness” of neutral dark matter.

Finally, CHAMPs are tightly coupled with baryons before its decay. Sigurdson & Kamionkowski (2004) assume $\theta_{\text{baryon}} = \theta_{\text{Ch}}$ where θ is the divergence of the fluid velocity. This approximation is valid when the Coulomb scattering between baryons and CHAMPs is efficient, i.e., CHAMPs and baryons are tightly coupled. However, the constraints from the Catalyzed BBN essentially allow only heavy CHAMP with $m_{\text{Ch}} \gtrsim 10^6 \text{ GeV}$ for $\tau_{\text{Ch}} \gtrsim 10^3 \text{ sec}$. It is unclear if the Coulomb scattering between baryons and such heavy CHAMPs is efficient. We have calculated the scattering efficiency and found that the tightly coupled approximation is indeed valid through the epoch of interest for $m_{\text{Ch}} \lesssim 10^8 \text{ GeV}$. The details of the calculations are found elsewhere (Kamada et al.). In the following, we adopt the formulation given by Sigurdson & Kamionkowski (2004) using the tightly coupled approximation between baryons and CHAMPs.

We modify CAMB (Lewis et al. 2000) to follow the evolution of density fluctuations in the Long-Lived CHAMP model. The basic equations are given in Sigurdson & Kamionkowski (2004). We obtain the power spectra for several τ_{Ch} s (see Eq. (10)). We find that the CHAMP matter power

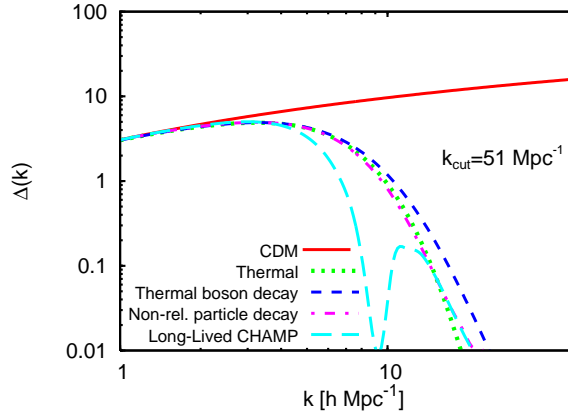


Fig. 2.— We plot the dimensionless linear matter power spectrum in Long-Lived CHAMP model ($\tau \simeq 2.5\text{yr}$). We compare it with the same dimensionless linear matter power spectra in the WDM models as in Fig. 1. The oscillation around $k \sim 9 h \text{ Mpc}^{-1}$ is the imprint of the “acoustic damping”.

spectrum is very similar to the WDM models, as seen in Fig. 2, when k_{Ch} is set such that

$$k_{\text{cut}} \equiv k_{\text{J}} \simeq 45 k_{\text{Ch}}. \quad (11)$$

Hereafter, we use k_{cut} defined in the above as a characteristic parameter of the models we consider. The corresponding lifetime of CHAMP is $\tau_{\text{Ch}} \simeq 2.5\text{yr}$ in the figure. The imprint of the CHAMP “acoustic damping” on the linear matter power spectra is clearly seen. One can naively guess that structures in the Long-Lived CHAMP model would be similar to those in the WDM models. It is important to study the non-linear growth of the matter distributions in the Long-Lived CHAMP model. We use large cosmological N -body simulations to this end.

3. Numerical simulations

Our simulation code is the parallel Tree-Particle Mesh code, **GADGET-2** (Springel 2005). We use $N = 512^3$ particles in a comoving volume of $L = 10 h^{-1} \text{ Mpc}$ on a side. The mass of a simulation particle is $5.67 \times 10^5 h^{-1} M_{\text{sun}}$ and the gravitational softening length is $1 h^{-1} \text{ kpc}$. We run a friends-of-friends (FoF) group finder (Davis et al. 1985) to locate groups of galaxies. We also identify substructures (subhalos) in each FoF group using SUB-FIND algorithm developed by Springel et al. (2001). We do not assign any thermal velocity to simulation particles because it can lead to formation of spurious objects (Colín et al. 2008). We start our simulation from relatively low redshift $z = 19$, at which the thermal motion of WDM is redshifted and negligible. It should be noted that the heavy, neutral dark matter produced by the CHAMP decay is assumed to have negligible thermal velocities.

In Fig. 3, we plot the projected matter distribution in the CDM model (left panel), in the

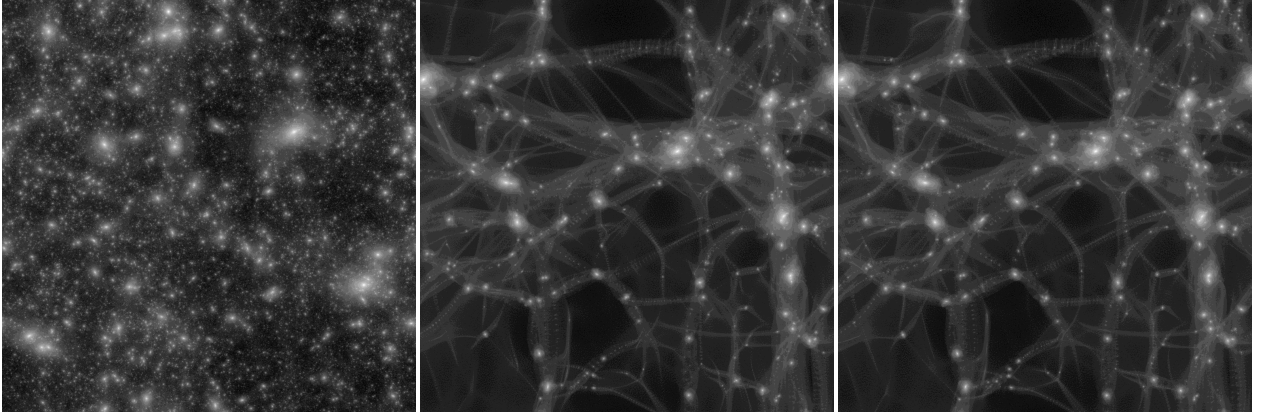


Fig. 3.— The projected matter distribution in the CDM model (left panel), in the Thermal WDM model (middle panel) and in the Long-Lived CHAMP model (right panel). For the Thermal WDM model and for the Long-Lived CHAMP model, we take the same cut-off scale $k_{\text{cut}} = 51 \text{ Mpc}^{-1}$ as in Fig. 2. One side of the plotted region is $L = 10 h^{-1} \text{ Mpc}$. Brighter regions denote higher matter densities.

Thermal WDM model (see subsection 2.1) (middle panel) and in the Long-Lived CHAMP model (right panel). For the Thermal WDM model and for the Long-Lived CHAMP model, we set the same cut-off scale $k_{\text{cut}} = 51 \text{ Mpc}^{-1}$ as in Fig. 2. One side of the plotted region is $10 h^{-1} \text{ Mpc}$. Regions with high matter densities appear bright in the plot. We see that many small objects, i.e., halos and subhalos, have formed in the CDM model. Contrastingly, in the Thermal WDM model and in the Long-Lived CHAMP model, the matter distribution is much smoother and appears more filamentary. The abundance of small objects is much reduced. Overall, the matter distributions in the Thermal WDM model and in the Long-Lived CHAMP model look similar. Note that numerous small objects along the filaments in the Thermal WDM model and in the Long-Lived CHAMP model could be numerical artifacts; this is a long-standing problem of hot/warm dark matter simulations due to discreteness effects (Wang & White 2007; Polisensky & Ricotti 2011). Earlier studies propose a simple formula for the critical halo mass,

$$M_c = 10.1 \times \rho_M d_{\text{mean}} k_{\text{peak}}^{-2}. \quad (12)$$

below which the abundance of halos is unreliable. Here, $d_{\text{mean}} = L/N^{1/3}$ is the mean comoving distance between simulation particles and k_{peak} is the wavenumber at the maximum of the $\Delta(k)$. We will discuss this point further in the following section.

We compare the halo mass functions in the models we consider in Fig. 4. The fiducial cut-off scale is $k_{\text{cut}} = 51 \text{ Mpc}^{-1}$ (left panel) as in Fig. 2, but we also show the results for $k_{\text{cut}} = 410 \text{ Mpc}^{-1}$ (right panel). The latter corresponds to $m_{3/2} \simeq 9.5 \text{ keV}$ for the thermally-produced gravitino WDM (see subsection 2.1) and $\tau_{\text{Ch}} \simeq 0.04 \text{ yr}$ for the Long-Lived CHAMP model. The halo mass M corresponding to k_{cut} is given by

$$M = \frac{4\pi G \rho_M}{3} \left(\frac{2\pi}{k_{\text{cut}}} \right)^3 \simeq 2 \times 10^9 h^{-1} M_{\text{sun}} \times \left(\frac{51 \text{ Mpc}^{-1}}{k_{\text{cut}}} \right)^3. \quad (13)$$

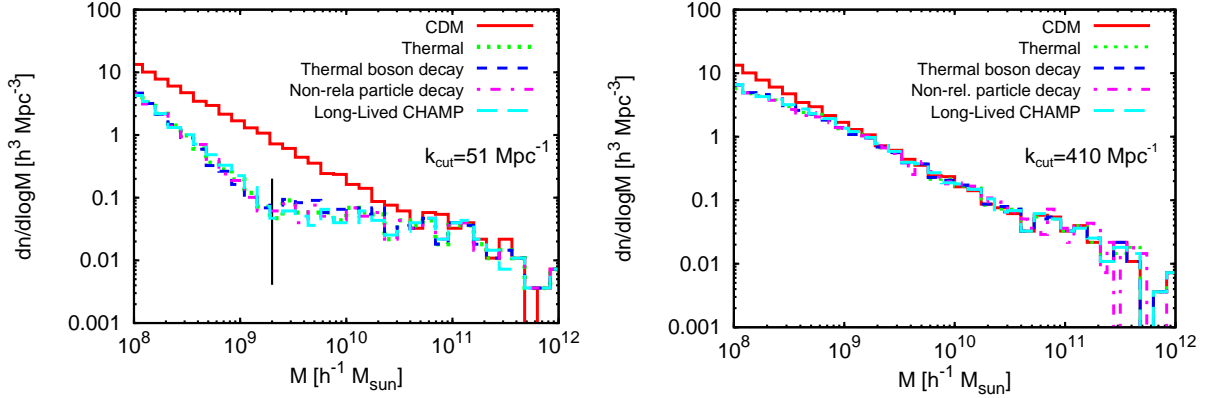


Fig. 4.— The halo mass functions in the CDM model, in the three WDM models and in the Long-Lived CHAMP model with $k_{\text{cut}} = 51 \text{ Mpc}^{-1}$ (left panel) and with $k_{\text{cut}} = 410 \text{ Mpc}^{-1}$ (right panel). The upturn at the halo mass $M \sim 2 \times 10^9 h^{-1} M_{\text{sun}}$ (vertical line) in the left panel may be owing to the artificial objects due to the discreteness effects.

distance from the center	0 – 50	50 – 100	100 – 150	150 – 200
number of satellites	19.7	15.62	8.08	14.16

Table 1: The number of observed satellites in each 50 kpc from the center of our Milky Way. According to Polisensky & Ricotti (2011), we count observed satellites known before the SDSS as one and those found by the SDSS as 3.54 due to the limited sky coverage of SDSS.

It is important to examine if the halo abundance is compromised by the above-mentioned numerical artifacts. For $k_{\text{cut}} = 51 \text{ Mpc}^{-1}$, we see upturns in the mass functions at $M \sim 2 \times 10^9 h^{-1} M_{\text{sun}}$. This is owing to peculiar discreteness effects in hot/warm dark matter simulations (Wang & White 2007; Polisensky & Ricotti 2011). The critical halo mass (see Eq. (12)) is $M_c \simeq 2 \times 10^9 h^{-1} M_{\text{sun}}$ for our simulation parameters $L = 10 h^{-1} \text{ Mpc}$, $N = 512^3$ and $k_{\text{peak}} \simeq 3 \text{ Mpc}^{-1}$ (see Fig. 2). The estimated mass limit is indeed consistent with the upturn seen in the left panel of Fig. 4.

Therefore, we conservatively restrict our discussion to halos with masses $M > M_c = 2 \times 10^9 h^{-1} M_{\text{sun}}$ for $k_{\text{cut}} = 51 \text{ Mpc}^{-1}$. The number of halos at $M \sim M_c$ in the three WDM models and in the Long-Lived CHAMP model is ~ 10 times smaller than that in the CDM model. Note the similarity of the halo abundances in the three WDM models and in the Long-Lived CHAMP model, as naively expected from the similarity in the linear matter power spectra.

In order to see if the WDM models and the Long-Lived CHAMP model resolve the “missing satellite problem”, we select Milky Way-size halos with masses of $0.5 \times 10^{12} h^{-1} M_{\text{sun}} < M_{\text{halo}} < 1.5 \times 10^{12} h^{-1} M_{\text{sun}}$ in our simulations. Although the halo mass of Milky Way itself is in debate (e.g. Xue et al. (2008) and references therein), we take a relatively lower mass among suggested values. For a (slightly) small value of M_{halo} , the relative mass ratio $M_{\text{satellite}}/M_{\text{halo}}$ becomes larger.

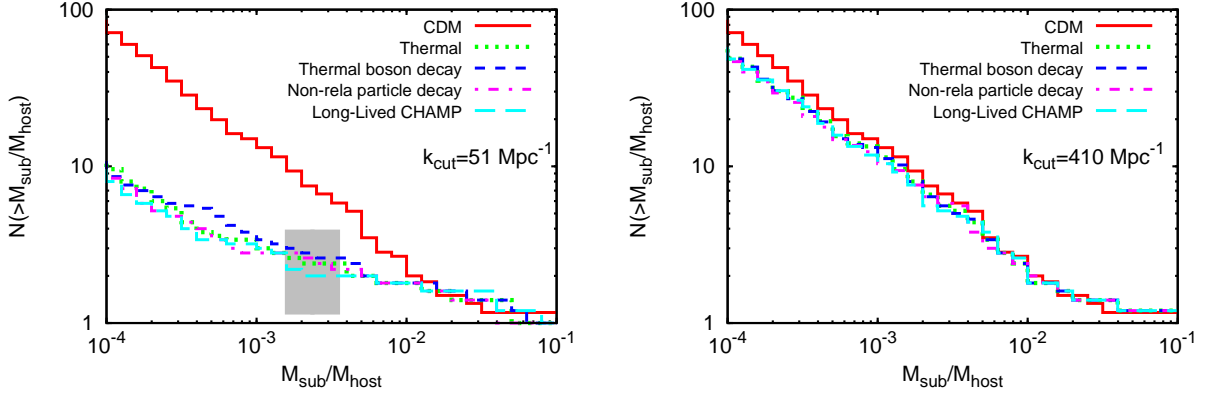


Fig. 5.— The cumulative subhalo mass functions averaged over Milky Way-size halos in the CDM model, in the three WDM models and in the Long-Lived CHAMP model with $k_{\text{cut}} = 51 \text{ Mpc}^{-1}$ (left panel) and with $k_{\text{cut}} = 410 \text{ Mpc}^{-1}$ (right panel). The shaded region corresponds to the mass of nonlinear objects at which the upturn (numerical artifacts) occurs in halo mass function (see the vertical line in the left panel of Fig. 4).

Then the apparent discrepancy between the number of observed satellites and the simulated subhalo abundance at a given mass scale becomes smaller. We thus choose the small Milky Way mass as a “conservative” one.

We compare the cumulative subhalo mass functions averaged over the Milky Way-size halos in our five models in Fig. 5. Note that we see again an upturn for $k_{\text{cut}} = 51 \text{ Mpc}^{-1}$ around $M_{\text{sub}}/M_{\text{host}} \simeq 2 \times 10^{-3}$. Above the mass scale, where we can measure the mass function robustly, the subhalo abundance is suppressed by a factor of ~ 10 in the models with $k_{\text{cut}} = 51 \text{ Mpc}^{-1}$ (left panel) compared with the CDM model. For the models with $k_{\text{cut}} = 410 \text{ Mpc}^{-1}$ (right panel), the subhalo abundance is suppressed at most by a factor of ~ 2 .

Let us now examine the radial distribution of the subhalos in our simulated Milky Way-size halos. We adopt the abundance of observed satellites in our Milky Way listed in Table 1. We account for the sky coverage of SDSS as follows. We count the number of the observed satellites in each 50 kpc bin such that each satellite known before the Sloan Digital Sky Survey (SDSS) is weighted as one whereas each satellite discovered by the SDSS is weighted as 3.54 (Polisensky & Ricotti 2011).

In Fig. 6, we compare the averaged radial distributions of the subhalos in the Milky Way-size halos. The left panel shows the radial distribution in the CDM model and the right panel shows the radial distribution in the Thermal WDM model with $k_{\text{cut}} \simeq 810 \text{ Mpc}^{-1}$, which corresponds to $m_{3/2} \simeq 16 \text{ keV}$ for the thermally-produced gravitino WDM. We include all the subhalos with $M > 2 \times 10^7 h^{-1} M_{\text{sun}}$. We also show variation of the radial distribution by thin solid lines. It should be noted that we set the gravitational softening length to be $1 h^{-1} \text{ kpc}$. The subhalo count in the innermost bin could have been affected by the spatial resolution. We can see the CDM model predicts a larger number of subhalos by a factor of 2 – 10 in each radial bin than observed. Note

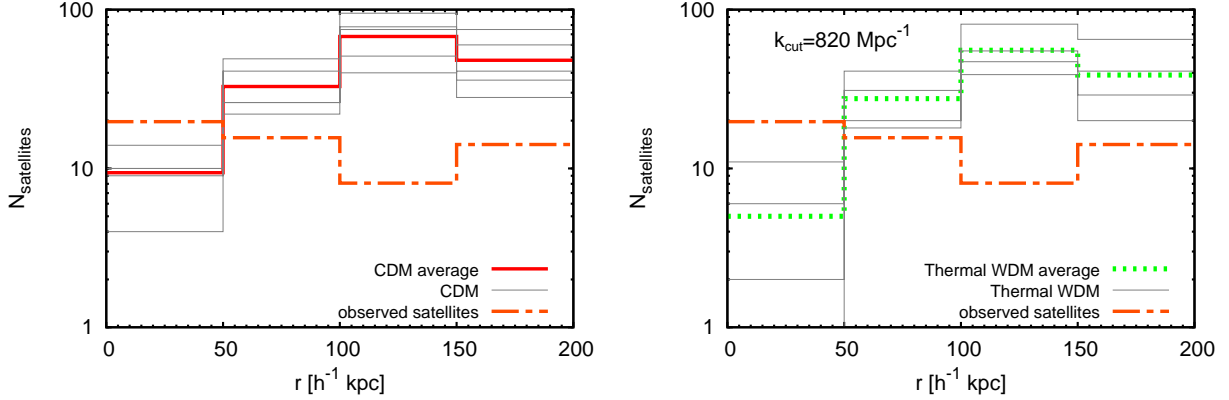


Fig. 6.— The radial distributions of subhalos in Milky Way-size halos in the CDM model (right panel) and in the Thermal WDM models (left panel) with $k_{\text{cut}} \simeq 810 \text{ Mpc}^{-1}$. We divide the distance from the center of host halo in 50 kpc bins. Each thin line corresponds to the radial distribution in each Milky Way-size halo. Thick lines represent the average over the Milky Way-size halos. For comparison, we also plot the radial distribution of the observed satellites listed in Table 1.

also that the number of satellites roughly scales with the host halo mass. Among the five Milky Way-size halos we selected, which have masses of $0.5 \times 10^{12} h^{-1} M_{\text{sun}} < M_{\text{halo}} < 1.5 \times 10^{12} h^{-1} M_{\text{sun}}$, the total number of subhalos differs by a factor of ~ 3 . By comparing the two panels in Fig. 6, we find that the radial distribution of subhalos in the Thermal WDM model with $k_{\text{cut}} \simeq 810 \text{ Mpc}^{-1}$ is similar to the one in CDM model and hence, the Thermal WDM model with $k_{\text{cut}} \simeq 810 \text{ Mpc}^{-1}$ does not seem to resolve the “missing satellite problem”.

We plot the subhalo radial distribution in the Thermal WDM model with $k_{\text{cut}} \simeq 51 \text{ Mpc}^{-1}$ in Fig. 7. For this model, where the suppression of the subgalactic-scale structure is most significant, a sizeable fraction of subhalos have masses smaller than M_c (see Eq. (12)). Thus the number count in the radial distribution is likely unreliable. Note however that, even without discarding the small mass subhalos ($M_{\text{sub}} < M_c$), the subhalo abundance is slightly smaller than the observed satellites.

We plot the radial distributions of subhalos with masses $M > M_c \simeq 10^8 h^{-1} M_{\text{sun}}$ in the Thermal WDM model with $k_{\text{cut}} \simeq 410 \text{ Mpc}^{-1}$ in Fig. 8. For this model, discarding small subhalos ($M_{\text{sub}} < M_c \simeq 10^8 h^{-1} M_{\text{sun}}$) reduces the subhalo abundance by a factor of ~ 2 . Overall, the radial distribution of subhalos (after discarding) appears to reproduce the observed distribution.

Let us now examine closely the similarity of the three WDM models and the Long-Lived CHAMP model when the characteristic cut-off scale k_{cut} is kept the same. We compare the averaged radial distributions of the subhalos in these models for $k_{\text{cut}} \simeq 410 \text{ Mpc}^{-1}$ (again after discarding small subhalos) and for $k_{\text{cut}} \simeq 810 \text{ Mpc}^{-1}$ in Fig. 9. From Fig. 4, Fig. 5 and Fig. 9, we conclude that the similar cut-off scale in the linear matter power spectra yields also similar halo and subhalo abundances and radial distributions.

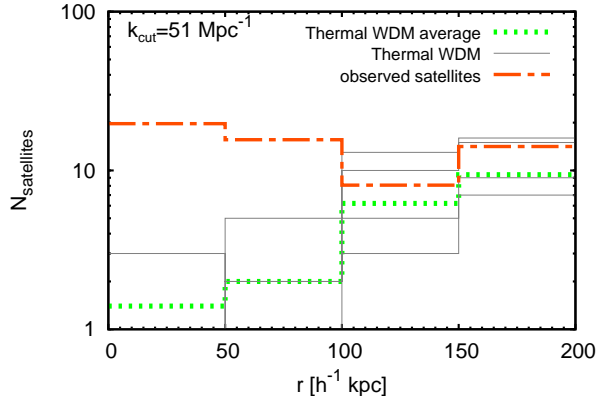


Fig. 7.— The radial distribution of subhalos in Milky Way-size halo in the Thermal WDM model with $k_{\text{cut}} = 51 \text{ Mpc}^{-1}$. This subhalos may include the artificial small objects due to the discreteness effects.

4. Summary

In this paper, we study the formation of non-linear objects in three WDM models and in a Long-Lived CHAMP model. We calculate the time evolution of the matter density fluctuations in the linear evolution regime by suitably modifying the public software **CAMB**. By using the obtained linear matter power spectra as initial conditions, we also perform large cosmological N -body simulations. The results are summarized as follows.

First, the comoving Jeans scale at the matter-radiation equality characterizes the linear matter power spectra of WDM models well. In the three WDM models motivated by particle physics, WDM particles are produced in different ways, but the linear matter power spectra with the same Jeans scale are very similar except for some difference at the damping tail at large k . We also consider a Long-Lived CHAMP model which has been suggested to yield a cut-off of the matter power spectrum through the “acoustic damping”. The cut-off scale of the matter power spectrum in the Long-Lived CHAMP model is determined by the comoving horizon scale when CHAMP decays. We empirically find the correspondence of the cut-off scales k_{cut} (see Eq. (11)) between the three WDM models and the Long-Lived CHAMP model.

By performing large cosmological N -body simulations, we compare the abundances of nonlinear halos and subhalos and the radial distributions of the subhalos in Milky Way-size halos. The three WDM models and the Long-Lived CHAMP model produce very similar halo and subhalo mass functions and radial distributions if k_{cut} is kept the same. Therefore, we conclude that k_{cut} determines the clustering property of WDM and Long-Lived CHAMP well in both linear and non-linear growth of the matter density.

One might naively guess that our simulation results for small non-linear objects may be compromised by numerical effects. However, our conclusions are drawn after discarding small objects

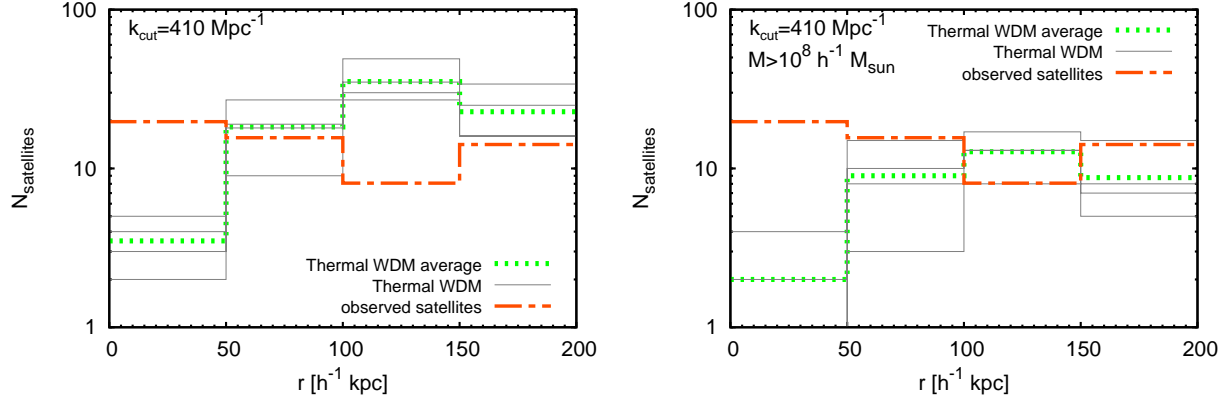


Fig. 8.— The same plot as Fig. 7 in the Thermal WDM model with $k_{\text{cut}} = 410 \text{ Mpc}^{-1}$. After discarding small subhalos ($M_{\text{sub}} < M_c \simeq 10^8 h^{-1} M_{\text{sun}}$), the subhalo abundance is reduced by a factor of ~ 2 (right panel).

that are likely numerical artifacts. We also compare the subhalo radial distributions in Milky Way-size halos with that of the observed satellites. We find that the WDM models and the Long-Lived CHAMP model are broadly consistent with the observation when they have $k_{\text{cut}} \sim 50 - 800 \text{ Mpc}^{-1}$. This cut-off scale corresponds to $m_{3/2} \sim 2 - 16 \text{ keV}$ for the thermally-produced gravitino WDM and $\tau_{\text{Ch}} \sim 0.01 - 2.5 \text{ yr}$ for the Long-Lived CHAMP. Because there is significant variation of the subhalo abundance among host halos with different masses, as reported by Ishiyama et al. (2009), it would be important to use a large sample of halos in order to address the validity of the models in a statistically complete manner.

Our results have a further implication for particles physics. We clarified how to put constraints on a few parameters of particles physics models which provide a WDM candidate. By calculating and comparing two quantities, the relic density of dark matter and the comoving Jeans scale at the matter-radiation equality, one can apply the reported constraints in a specific particle physics model (e.g. the mass of thermally-produced gravitino WDM or sterile neutrino WDM produced through the Dodelson & Widrow (1994) mechanism) to virtually any model parameters of interest.

Finally, we note that the so-called astrophysical feedback processes are also thought to affect the abundance of luminous satellite galaxies (Brooks et al. 2012). Unfortunately, whether or not and how the baryonic processes changes our simple understanding based on the cut-off scale $k_{\text{cut}} \sim 50 - 800 \text{ Mpc}^{-1}$ is unclear due to the complexity of the baryonic processes. Regarding “missing satellite problem”, both WDM and Long-Lived CHAMP models and the baryon feedback may explain the small number of the observed luminous satellites. The degeneracy can be resolved, in principle, by the direct probes of non-luminous small objects, by, for instance, future submillilensing surveys (Hisano et al. 2006).

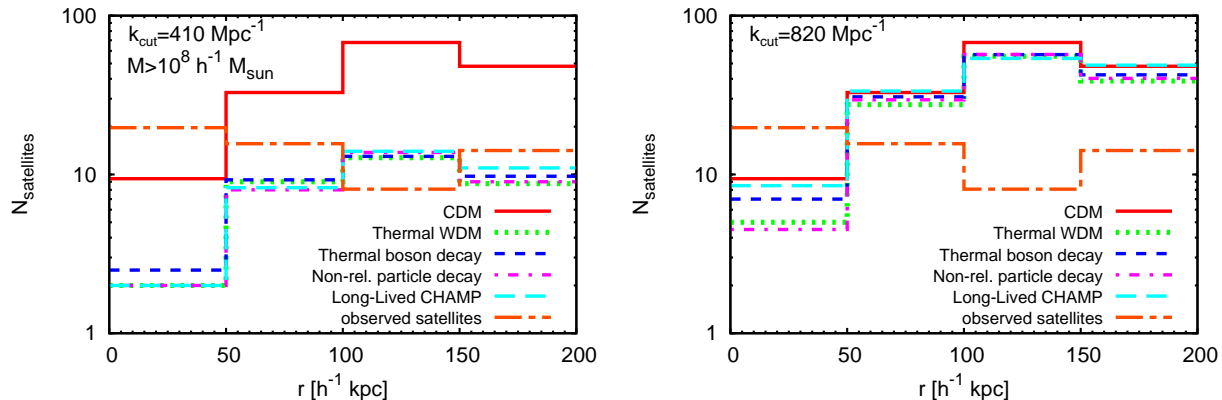


Fig. 9.— Comparison of the averaged radial distributions in the CDM model, in the three WDM models and in the Long-Lived CHAMP model for $k_{\text{cut}} \simeq 410 \text{ Mpc}^{-1}$ (left panel) and for $k_{\text{cut}} \simeq 820 \text{ Mpc}^{-1}$ (right panel). For $k_{\text{cut}} \simeq 410 \text{ Mpc}^{-1}$ (left panel), we have discarded small subhalos ($M_{\text{sub}} < M_c \simeq 10^8 h^{-1} M_{\text{sun}}$) as in Fig. 8.

5. Acknowledgement

This work is supported in part by JSPS Research Fellowship for Young Scientists (A.K.), by Grant-in-Aid for the Ministry of Education, Culture, Sports, Science and Technology, Government of Japan Nos. 21111006, 22244030, 23540327 (K.K.), 23740195 (T.T.) and by World Premier International Research Center Initiative, MEXT, Japan. Numerical computation in this work was carried out in part at the Yukawa Institute Computer Facility.

REFERENCES

- Aoyama, S., Ichiki, K., Nitta, D., & Sugiyama, N. 2011, *J. Cosmology Astropart. Phys.*, 9, 25
- Barkana, R., Haiman, Z., & Ostriker, J. P. 2001, *ApJ*, 558, 482
- J. Beringer *et al.* [Particle Data Group Collaboration], 2012, *Phys. Rev. D*, 86, 010001
- Bode, P., Ostriker, J. P., & Turok, N. 2001, *ApJ*, 556, 93
- Boyanovsky, D. 2008, *Phys. Rev. D*, 78, 103505
- Boyarsky, A., Lesgourgues, J., Ruchayskiy, O., & Viel, M. 2009, *J. Cosmology Astropart. Phys.*, 5, 12
- Boylan-Kolchin, M., Bullock, J. S., & Kaplinghat, M. 2011, *MNRAS*, 415, L40
- Boylan-Kolchin, M., Bullock, J. S., & Kaplinghat, M. 2012, *MNRAS*, 422, 1203
- Brooks, A. M., Kuhlen, M., Zolotov, A., & Hooper, D. 2012, arXiv:1209.5394

- Buchmüller, W., Covi, L., Kersten, J., & Schmidt-Hoberg, K. 2006, *J. Cosmology Astropart. Phys.*, 11, 7
- Cembranos, J. A. R., Feng, J. L., Rajaraman, A., & Takayama, F. 2005, *Physical Review Letters*, 95, 181301
- Cline, J. M. 1992, *Physical Review Letters*, 68, 3137
- Colín, P., Valenzuela, O., & Avila-Reese, V. 2008, *ApJ*, 673, 203
- Cyburt, R. H., Ellis, J., Fields, B. D., Olive, K. A., & Spanos, V. C. 2006, *J. Cosmology Astropart. Phys.*, 11, 14
- Davis, M., Efstathiou, G., Frenk, C. S., & White, S. D. M. 1985, *ApJ*, 292, 371
- Dine, M., Nelson, A. E., Nir, Y., & Shirman, Y. 1996, *Phys. Rev. D*, 53, 2658
- Dodelson, S., & Widrow, L. M. 1994, *Physical Review Letters*, 72, 17
- Dunstan, R. M., Abazajian, K. N., Polisensky, E., & Ricotti, M. 2011, *arXiv:1109.6291*
- Endo, M., Hamaguchi, K., & Takahashi, F. 2006, *Physical Review Letters*, 96, 211301
- Gao, L., & Theuns, T. 2007, *Science*, 317, 1527
- Gondolo, P., & Gelmini, G. 1991, *Nuclear Physics B*, 360, 145
- Griest, K., & Seckel, D. 1991, *Phys. Rev. D*, 43, 3191
- Hamaguchi, K., Hatsuda, T., Kamimura, M., Kino, Y., & Yanagida, T. T. 2007, *Physics Letters B*, 650, 268
- Hisano, J., Kohri, K., & Nojiri, M. M. 2001, *Physics Letters B*, 505, 169
- Hisano, J., Inoue, K. T., & Takahashi, T. 2006, *Physics Letters B*, 643, 141
- Hu, W., & Silk, J. 1993, *Physical Review Letters*, 70, 2661
- Ibe, M., Sato, R., Yanagida, T. T., & Yonekura, K. 2011, *Journal of High Energy Physics*, 4, 77
- Ibe, M., & Sato, R. 2012, *arXiv:1204.3499*
- Ishiyama, T., Fukushima, T., & Makino, J. 2009, *ApJ*, 696, 2115
- Jedamzik, K. 2008, *Phys. Rev. D*, 77, 063524
- Jedamzik, K. 2008, *J. Cosmology Astropart. Phys.*, 3, 8
- Jittoh, T., Kohri, K., Koike, M., et al. 2011, *Phys. Rev. D*, 84, 035008

- Kaplinghat, M. 2005, *Phys. Rev. D*, 72, 063510
- Kaplinghat, M., & Rajaraman, A. 2006, *Phys. Rev. D*, 74, 103004
- Kamada, A., et al. in progress
- Kamimura, M., Kino, Y., & Hiyama, E. 2009, *Progress of Theoretical Physics*, 121, 1059
- Kawasaki, M., Sugiyama, N., & Yanagida, T. 1997, *Modern Physics Letters A*, 12, 1275
- Kawasaki, M., Kohri, K., & Moroi, T. 2001, *Phys. Rev. D*, 63, 103502
- Kawasaki, M., Takahashi, F., & Yanagida, T. T. 2006, *Phys. Rev. D*, 74, 043519
- Kawasaki, M., Kohri, K., & Moroi, T. 2007, *Physics Letters B*, 649, 436
- Kohri, K., & Takayama, F. 2007, *Phys. Rev. D*, 76, 063507
- Kohri, K., & Takahashi, T. 2010, *Physics Letters B*, 682, 337
- Komatsu, E., Smith, K. M., Dunkley, J., et al. 2011, *ApJS*, 192, 18
- Kravtsov, A. 2010, *Advances in Astronomy*, 2010,
- Kusenko, A. 2009, *Phys. Rep.*, 481, 1
- Lewis, A., Challinor, A., & Lasenby, A. 2000, *ApJ*, 538, 473
- Lewis, A., & Challinor, A. 2002, *Phys. Rev. D*, 66, 023531
- Lin, W. B., Huang, D. H., Zhang, X., & Brandenberger, R. 2001, *Physical Review Letters*, 86, 954
- Lovell, M. R., Eke, V., Frenk, C. S., et al. 2012, *MNRAS*, 420, 2318
- Ma, C.-P., & Bertschinger, E. 1995, *ApJ*, 455, 7
- Menci, N., Fiore, F., & Lamastra, A. 2012, *MNRAS*, 421, 2384
- Moore, B., Ghigna, S., Governato, F., et al. 1999, *ApJ*, 524, L19
- Olive, K. A., & Turner, M. S. 1982, *Phys. Rev. D*, 25, 213
- Papastergis, E., Martin, A. M., Giovanelli, R., & Haynes, M. P. 2011, *ApJ*, 739, 38
- Percival, W. J., Reid, B. A., Eisenstein, D. J., et al. 2010, *MNRAS*, 401, 2148
- Petraki, K., & Kusenko, A. 2008, *Phys. Rev. D*, 77, 065014
- Polisensky, E., & Ricotti, M. 2011, *Phys. Rev. D*, 83, 043506
- Pospelov, M. 2007, *Physical Review Letters*, 98, 231301

- Reid, B. A., Percival, W. J., Eisenstein, D. J., et al. 2010, MNRAS, 404, 60
- Schneider, A., Smith, R. E., Macciò, A. V., & Moore, B. 2012, MNRAS, 424, 684
- Shaposhnikov, M., & Tkachev, I. 2006, Physics Letters B, 639, 414
- Sigurdson, K., & Kamionkowski, M. 2004, Physical Review Letters, 92, 171302
- Springel, V. 2005, MNRAS, 364, 1105
- Springel, V., White, S. D. M., Tormen, G., & Kauffmann, G. 2001, MNRAS, 328, 726
- Steffen, F. D. 2007, SUSY06: The 14th International Conference on Supersymmetry and the Unification of Fundamental Interactions, 903, 595
- Strigari, L. E., Kaplinghat, M., & Bullock, J. S. 2007, Phys. Rev. D, 75, 061303
- Takahashi, F. 2008, Physics Letters B, 660, 100
- Tegmark, M., Strauss, M. A., Blanton, M. R., et al. 2004, Phys. Rev. D, 69, 103501
- Viel, M., Lesgourgues, J., Haehnelt, M. G., Matarrese, S., & Riotto, A. 2005, Phys. Rev. D, 71, 063534
- Wang, J., & White, S. D. M. 2007, MNRAS, 380, 93
- Xue, X. X., Rix, H. W., Zhao, G., et al. 2008, ApJ, 684, 1143
- Yoshida, N., Sokasian, A., Hernquist, L., & Springel, V. 2003, ApJ, 591, L1
- Yue, B., & Chen, X. 2012, ApJ, 747, 127